33RD INTERNATIONAL COSMIC RAY CONFERENCE, RIO DE JANEIRO 2013
THE ASTROPARTICLE PHYSICS CONFERENCE

ICRC 2013

Characterization of the Optical and X-ray Properties of the Northwestern Wisps in the Crab Nebula

T. SCHWEIZER[1], N. BUCCIANTINI[2,6], W. IDEC[1,7], K. NILSSON[3], A. TENNANT[4], M.C. WEISSKOPF[4], R. ZANIN[5]

[1]*Max-Planck-Institute for Physics, Foehringer Ring 6, 80805 Munich, Germany*
[2]*INAF - Osservatorio Astrofisico di Arcetri, L.go E. Fermi 5, 50125, Firenze, Italy*
[3]*Finnish Centre for Astronomy with ESO (FINCA), University of Turku, 20, FI-21500 , Finland*
[4]*Space Science Department, NASA Marshall Space Flight Center, ZP12, Huntsville, AL 35812*
[5]*Universitat de Barcelona, Departament d'Astronomia i Meteorologia, Spain*
[6]*INFN - Sezione di Firenze, Via G. Sansone 1, 50019 Sesto Fiorentino, Firenze, Italy*
[7]*Department of Astrophysics, University of Łódź, ul. Pomorska 149/153, 90-236 Łódź, Poland*

tschweiz@googlemail.com

Abstract: We have studied the wisps to the northwest of the Crab pulsar as part of a multiwavelength campaign in the visible and in X-rays. Optical observations were obtained using the Nordic Optical Telescope in La Palma and X-ray observations were made with the Chandra X-ray Observatory. The observing campaign took place from October 2010 until September 2012. About once per year we observe wisps forming and peeling off from (or near) the region commonly associated with the termination shock of the pulsar wind. We find that the exact locations of the northwestern wisps in the optical and in X-rays are similar but not coincident, with X-ray wisps preferentially located closer to the pulsar. This suggests that the optical and X-ray wisps are not produced by the same particle distribution. Our measurements and their implications are interpreted in terms of a Doppler-boosted ring model that has its origin in MHD modeling. While the Doppler boosting factors inferred from the X-ray wisps are consistent with current MHD simulations of PWNe, the optical boosting factors are not, and typically exceed values from MHD simulations by about a factor of 3.

Keywords: ISM: supernova remnants - pulsars: individual: Crab - radiation mechanisms: non-thermal - ISM: supernova remnants: individual: Crab Nebula

1 Introduction

The Crab Nebula is one of the most studied targets in the sky as it is bright and observable over a very broad spectral range. The Nebula is a remnant from a supernova explosion that was observed on earth in 1054 C.E. Located at a distance of $\sim$2 kpc, the system is powered by a pulsar of spin-down luminosity $L \sim 5 \times 10^{38}$ erg s^{-1} and period $P \sim 34$ ms. The history and general properties of the system are nicely summarized in the review by [1].

The discovery of γ-ray flaring in 2010 September [2, 3] stimulated a renewed interest in the Crab Nebula. In this work we focus on the properties and time evolution of variable "wisp" structure observed to the north-west of the pulsar in the inner nebula. We present the results of two observing campaigns, one in the visible and one in X-rays.

2 The observations

2.1 The optical observations

Optical data was obtained using the 2.56m Nordic Optical Telescope (NOT) located in the Observatorio del Roque de los Muchachos on the island of La Palma. 24 images were taken from November 2010 until September 2012 using the Andalucia Faint Object Spectrograph and Camera (ALFOSC). Fig. 1 shows one of the 24 optical images.

2.2 The X-ray observations

Subsequent to the discovery of γ-ray flaring in 2010 September [2, 3] a series of Chandra X-ray Observatory observations was initiated on approximately a monthly cadence. Chandra observations have continued, now as part of the Chandra general observer program, yielding a sequence which covers approximately two years. As with our optical observations, the coverage is not continuous. Since Chandra is not allowed to point within 45$^{\rm o}$ of the Sun, there is a 90 day interval during the summer when the Crab may not be observed.

3 Data analysis

Images were analyzed to characterize the shape of the wisps in both the radial direction from the pulsar and angular extent about the pulsar. Our analysis to determine the radial distribution through the wisps restricted data to the narrow $3''$ wide strip shown in Fig. 1. Optical and X-ray data were binned in radial bins of $0.11''$ and $0.492''$ respectively. For azimuthal distributions we utilized $0.5''$-wide elliptical annuli, on the sky and centered on the peak of the radial distribution.

3.1 Analysis of the radial and azimuthal profiles of the wisps

For the radial profiles, in both optical and X-ray, we fit each brightness profile to a constant plus to a series of Gaussians. Initially a Gaussian is located at each peak seen in the profile. The model was then fit using a least squares fitting method that allowed all parameters to vary. After the fit had converged, we then visually inspected to ensure the main peaks had been properly located and if not the model would

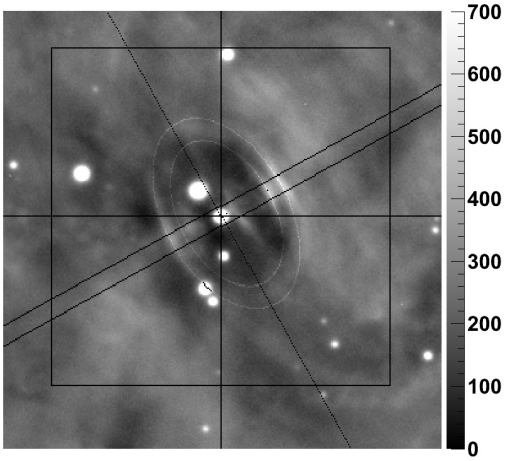

Figure 1: Optical image of the inner portion of the Crab Nebula taken on 13th of April 2011 (during a γ-ray flare [4]) covering $50'' \times 50''$ field of view. North is up and east is to the left. The two parallel lines at a position angle of 119° measured east from north outline the region used to measure radial profiles. Two ellipses passing through the wisps at $8.0''$ and $10.1''$ north-west of the pulsar are shown. The aspect ratio of the ellipses is 0.6 and their center is offset from the pulsar by $0.8''$ to the NW. The intensity units are arbitrary.

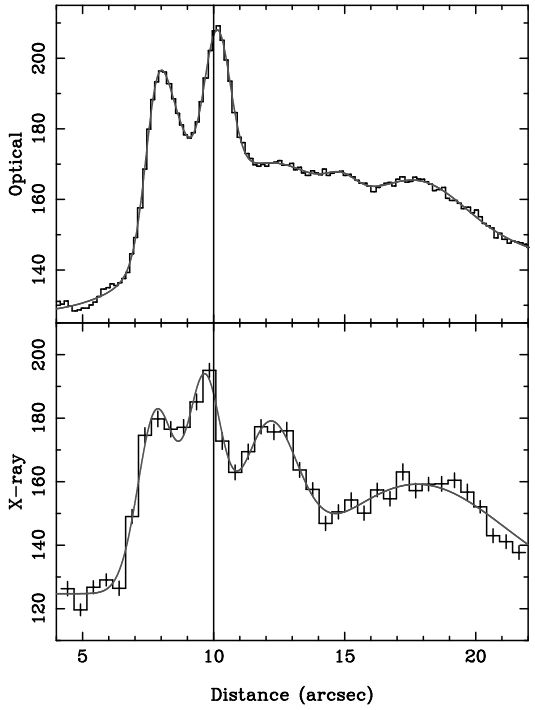

Figure 2: The upper panel shows the radial brightness distribution for the optical data for April 13, 2011 ($\mu Jy/arcsec^2$). The bottom panel is the corresponding X-ray radial distribution for the average from April 14 until April 28, 2011 (counts per ACIS pixel). The solid lines are a model fit based on a number of Gaussians. The vertical line at $10''$ is drawn to emphasize that the optical and X-ray peaks do not exactly coincide.

be modified, either by adjusting parameter values or adding an additional Gaussian, and then refit.

An example of an optical and an X-ray radial profile measured close in time is shown Fig. 2. We see two prominent peaks in the optical and the presence of at least three peaks in the X-ray profile. In general, the peak closest to the pulsar is most usually identified with the location of the termination shock. Fig. 2 demonstrates that the X-ray peak at $10''$ is located at a slightly different (and smaller) distance than the peak in the optical. The exposures in optical and X-rays in the figure are not precisely simultaneous and the average time difference is about 8 days. However, even if we account for the apparent radial motion (§ 3.2), the X-ray wisp is still closer to the pulsar than the nearest optical wisp.

We measure also azimuthal profiles of the wisps, which have ellipse-like shape in the azimuthal direction due to the fact, that they are presumably produced in a ring shape in the equatorial plane of the pulsar. In the X-ray the innermost ellipse has an aspect-ratio of 0.49 and the pulsar features an offset of $\approx 0.9''$ below the plane of the wisp.

We find that azimuthal profiles for optical and X-ray differ from each other. The former has a sharper peak than the latter and the FWHM in optical is around 30^o while in X-ray around 70^o.

3.2 The radial evolution of the wisps as a function of time

Fig. 3 is a graphical representation showing most of the optical and X-ray radial projections as a function of the angular distance from the pulsar. For display purposes only, low frequency terms have been subtracted. The algorithm applied was the TSpectrum background subtraction algorithm from the ROOT-package [5].

In Fig. 3 we also trace the outward motion of a particular peak by drawing a line through the position of what appears to be the same peak but at different times. There appears to be possibly 5 distinct progressions of peaks in the optical data and possibly 7 in X-rays. We have not attempted to connect progressions across summer gaps, but one could do so. As the slopes of the lines indicating the outward progression are different, so are the inferred velocities. We calculate the apparent velocity on the sky in $''/day$, and, assuming a distance of 2 kpc, the deprojected physical velocity. For deprojection we use an inclination angle of 57° [6]. For oprical and X-rays, we obtain the deprojected velocity value ranges (in the terms of v/c) of $0.21 - 0.44$ and $0.16 - 0.42$ respectively.

4 Model fitting and theoretical discussion

The MHD model developed with success in the past years [7, 8, 9, 10, 11, 12, 13] explains the existence of rings and wisps observed in pulsar wind nebulae (PWNe) in terms of axisymmetric enhancements of the emissivity immediately downstream of the termination shock.

A simplified model for a wisp can be built on the assumption that a wisp is due to a torus- or ring-like region within the nebula. This region is bright or dim depending

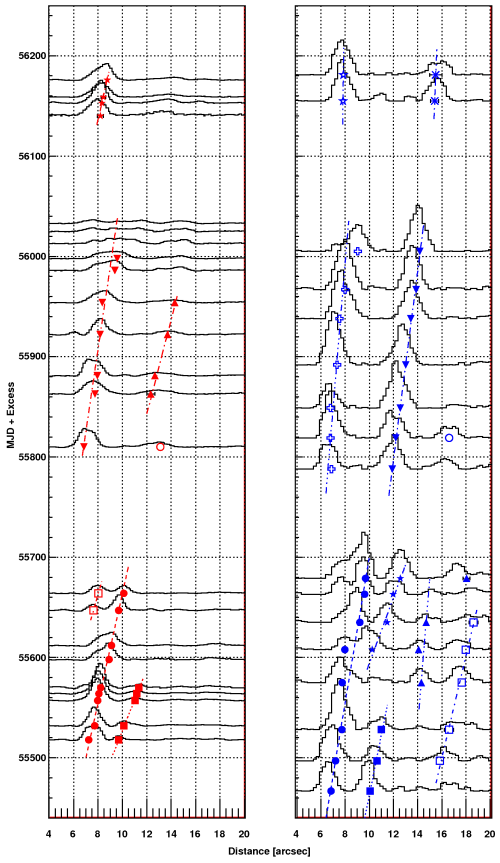

Figure 3: 23 optical and 17 X-ray radial profiles as a function of distance northwest of the pulsar (close in time observations are omitted for clarity). Symbols are placed on the distance axis to show the position of the peak of the Gaussian fitted to the original profile. The lines, simply best guesses, are an interpretation of the time evolution of the position of a particular peak.

on Doppler boosting due to the relative direction of the observer, and the particle flow. This boosted-ring model appears in alternative explanations for the origin of the wisps, e.g. in term of ion-cyclotron compression [14] or cooling instabilities [15]. The boosting is required in all of these models to explain the azimuthal luminosity profile of the wisps, and the fact that one side of the nebula (the front side) is brighter than the back side. This idea has been adopted in the past [16, 17, 18] to model the jet torus structure observed in X-rays in several PWNe, and to estimate typical flow speeds in these systems.

A wisp originates from a region shaped like a torus, with major radius R_o and a minor radius r_o. The ratio r_o/R_o we call the thickness of the torus. The plane of the torus has an inclination α with respect to the line of sight, which, within the axisymmetric approximation, is equal to the angle between the nebular axis and the plane of the sky. The fluid in the torus has a uniform flow speed V_{fl}, confined in meridianal planes (planes containing the nebular axis). The azimuthal component of this flow speed is assumed to be 0. V_{fl} forms an angle β with respect to the plane of the torus.

We fit the optical data to this model as follows:

- We select a set of input parameters r_o/R_o, α, β, and V_{fl}.
- An emission map is built (the emission is normalized to the maximum).
- The emission map is convolved with the point spread function of the observation.
- Emission profiles are extracted both along the wisp and along the axis of the nebula.
- The simulated radial and azimuthal profiles are added to an assumed background and then compared with the data. The background is based on a simple 2D polynomial least-squares fit, as shown in Fig 4.
- This procedure is repeated until a set of input parameters are found that provide a reasonable fit.

Fig. 4 shows a simulated map of one of the optical wisps made using the best fit input parameters.

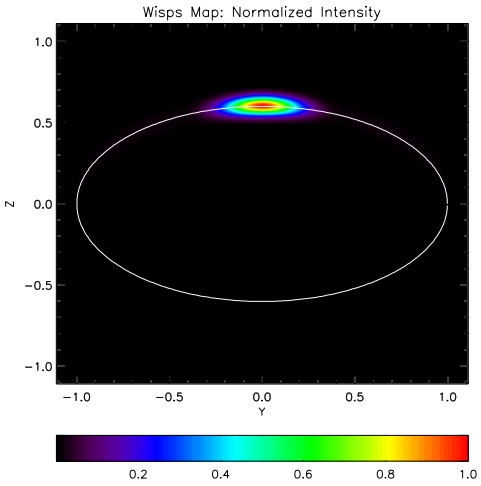

Figure 4: Simulated synchrotron map of the optical wisp for MJD=55532 and at a distance of 7.7″. The axes are in arbitrary units normalized to the wisp major radius R_o. Colors indicate the level of the flux, normalized to the maximum.

There are several interesting points to note:

- Typical flow speeds inferred from our model range between $V_{fl} = 0.8$c and $V_{fl} = 0.95$c. Using a chaotic magnetic field distribution leads to even higher velocities.
- The angle β is almost equal to the angle α.
- The wisps appear to be unresolved and the ratio r_o/R_o is less than 0.1.

The high values of the flow speed correspond to boosting factors that are in excess of typical values found in MHD simulations by about a factor between 2 and 5 depending on which initial value of β one chooses. This is related to the narrow extent of the optical wisps which fade to the sky background level within $\pm 20^\circ$ from the axis and to the fact that $\beta \approx \alpha$, implying that the flow speed on the front side of the nebula is directed toward the observer. It appears that the optical wisps are consistent with narrow features, possibly close to emitting sheets. It is also interesting to note that there is a trend in the observed flow speeds as a function of wisp location, with higher values for inner wisps, as shown in Fig. 5.

A comparison between the azimuthal profile in optical and X-rays has also been done. For the X-ray data, in order

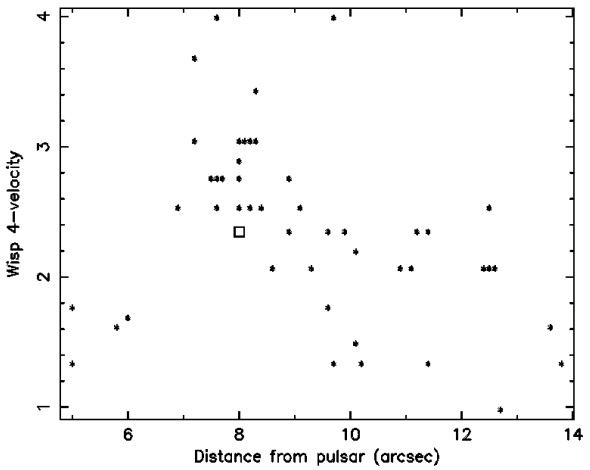

Figure 5: Boosting four-velocity $(V_{fl}/c)/\sqrt{[1-(V_{fl}/c)^2]}$ for the optical wisps as a function of their distance from the pulsar. The square denotes the boosting four-velocity obtained from the averaged optical profile. Note that the data points at radii $\leq 7''$ are most likely not due to wisps, but other optical features such as the halo [1].

to have sufficient statistics, instead of a single epoch, we consider an average over the entire set of observations and only for the inner (brighter) X-ray wisp region located $\sim 8''$ away from the pulsar. To eliminate the possibility that any possibly obtained difference is due to averaging the X-ray data, we also averaged the optical data over all of our epochs. The resulting model parameters are $r_o/R_o = 0.1$, $\alpha = \beta = 35^\circ$ both for optical and X-ray, while $V_{fl} = 0.6c \pm 0.1c$ for the X-ray and $V_{fl} = 0.91c \pm 0.03c$ for the optical. We may associate this with a boosting four-velocity $U_{fl} = (V_{fl}/c)/\sqrt{[1-(V_{fl}/c)^2]}$ of 0.75 for X-ray and 2.20 for optical (i.e. a factor of 3.13). Thus, we can safely conclude that the azimuthal extent of this X-ray wisp is larger than in the optical and, within the context of our model, this implies lower inferred speeds for the particles producing the X-rays. This leads to an evident conclusion that X-ray and optical wisps are not produced by the same particle distribution: they do not coincide in location or in terms of the degree of Doppler boosting.

5 Conclusions

The results of our study can be summarized in few points:

- We find that the optical and X-ray wisps appear in the intervals of $\approx$ 1y at the region which is believed to be the termination shock of the pulsar wind. The optical and X-ray wisps are physically separated. It is worth to notice, that optical and radio wisps are also separated from each other [19].
- The time interval of the γ-ray flares is coinciding with this of wisp formation, however the moment of wisp formation did not coincide wit the γ-ray flare of 2011 April.
- The wisps propagate outwards with velocities projected onto the sky ranging from ~ 0.1(v/c) to ~ 0.4(v/c). The velocities seem to increase with the increasing distance from the pulsar. This could be result of a re-acceleration mechanism, or (more likely) of a complicated 3D geometry.
- Within the context of an MHD model, we find that optical wisps are more strongly (by a factor of ~ 3) Doppler-boosted than the X-ray wisps. In particular, we found that the azimuthal luminosity profile of the X-ray wisps is fully compatible with typical boosting factors found in MHD simulations of PWNe. Instead, the azimuthal luminosity profile of the optical wisps requires particles velocities that are incompatible with the results of global numerical modeling of PWNe [7, 10]. This should be investigated with future modeling.
- The mentioned differences in the behavior and properties of the optical and X-ray wisps suggest that they are produced by different particle distributions, however originating from a common prompt.

Further information on our study can be found in the full article [20].

Acknowledgment: The optical observations used in this work have been done with the Nordic Optical Telescope, operated on the island of La Palma in the Observatorio del Roque de los Muchachos of the Instituto de Astrofisica de Canarias. The data were obtained [in part] with ALFOSC, provided by the Instituto de Astrofisica de Andalucia under a joint agreement with the University of Copenhagen and NOTSA. The staff at the NOT provided much useful support, particularly Thomas Augusteijn.

The X-ray observations have been done with the Chandra X-ray satellite. A.T. and M.C.W would like to acknowledge support from the Chandra Project. We would also like to acknowledge the Director of the Chandra Science Center for authorizing Director's Discretionary Time and Chandra Proposal 1350025 for the remainder of the observations.

References

[1] Hester J. J., 2008, ARA&A, 46, 127
[2] Tavani M. et al. 2011, Science, 331, 736
[3] Abdo A. A. et al. 2011, Science, 331, 739
[4] Buehler R., et al., 2012, ApJ, 749, 8
[5] Morháč M., Kliman J., Matoušek V., Veselský M., Turzo I., 1997, Nuclear Instruments and Methods in Physics Research A, 401, 113
[6] Weisskopf M. C., Elsner R. F., Kolodziejczak J. J., ODell S. L., Tennant A. F., 2012, ApJ, 746, 41
[7] Komissarov S. S., Lyubarsky Y. E., 2003, MNRAS, 344, L93
[8] Komissarov S. S., Lyubarsky Y. E., 2004, MNRAS, 349, 779
[9] Del Zanna L., Amato E., Bucciantini N., 2004, A&A, 421, 1063
[10] Bucciantini N., Arons J., Amato E., 2011, MNRAS, 410, 381
[11] Del Zanna L., Volpi D., Amato E., Bucciantini N., 2006, A&A, 453, 621
[12] Volpi D., Del Zanna L., Amato E., Bucciantini N., 2008, A&A, 485, 337
[13] Camus N. F., Komissarov S. S., Bucciantini N., Hughes P. A., 2009, MNRAS, 400, 1241
[14] Spitkovsky A., Arons J., 2004, ApJ, 603, 669
[15] Foy J. P., Hester J., 2009, in American Astronomical Society Meeting Abstracts #213 Vol. 41 of Bulletin of the American Astronomical Society, p. 488.01
[16] Romani R. W., Ng C.-Y., 2003, ApJ, 585, L41
[17] Ng C.-Y., Romani R. W., 2004, ApJ, 601, 479
[18] Romani R. W., Ng C.-Y., Dodson R., Brisken W., 2005, ApJ, 631, 480
[19] Bietenholz M. F., Hester J. J., Frail D. A., Bartel N., 2004, ApJ, 615, 794
[20] Schweizer T., Bucciantini N., Idec W., Nilsson K., Tennant A., Weisskopf M. C., Zanin R., `http://arxiv.org/abs/1301.1321`